encit 2020

ABCM
Associação Brasileira de Engenharia e Ciências Mecânicas

18th Brazilian Congress of Thermal Sciences and Engineering
November 16–20, 2020 (Online)

ENC-2020-0496
EVALUATION OF ZERO-DIMENSIONAL CO AND NO ENGINE EMISSIONS MODELS AND THEIR SUITABILITY FOR E10

Oswaldo M. França Jr.
Rogério G. dos Santos
Universidade Estadual de Campinas - Unicamp
o226857@g.unicamp.br
roger7@fem.unicamp.br

Clayton B. Zabeu
Instituo Mauá de Tecnologia
clayton@maua.br

Mario E. S. Martins
Universidade Federal de Santa Maria - UFSM
mario@mecanica.ufsm.br

Abstract. *Emissions standards are getting more stringent year after year, requiring greater development efforts. More and more emissions tests have to be ran, until the engine is sufficiently tuned for the market. On the other hand, building prototypes is very expensive. One way of reducing development costs and time is the use computer simulations. However, in order to predict emissions, more complex and computationally expensive methods are usually necessary, like three-dimensional (3D) computational fluid dynamics (CFD) coupled with chemical kinetics calculations. Such simulations can take very long, even for one single case, making them only worth it for conceptual development. This work aims at evaluating zero-dimensional (0D) kinetic emissions models and their suitability in predicting CO and NO exhaust emissions from combustion of E10 (a mixture of 10% ethanol with 90% gasoline). Test bench results from a 3 cylinder, 1.2 liter turbocharged direct injection spark ignition (DISI) engine, running on E10, were used as reference for evaluating model accuracy and suitability for this fuel. Although the model presented high deviations compared to measurements, over predicting CO and under predicting NO, results pointed out that the general trend for emissions, at full load and as function of engine speed, could be captured. Further model improvements would be possible through calibration of multiplier coefficients and the addition of a NO_2 kinetic model.*

Keywords: *engine, emissions, simulation*

1. INTRODUCTION

In an effort to mitigate the environment impact of the transportation sector, emissions regulations are getting more and more stringent with time (Vitesco Technologies, 2019), requiring greater development efforts. For instance, in order to tune a particular engine/vehicle combination to the market, several emissions tests must be ran, each of which taking up to 12 hours between soak and preparation (ABNT, 2012).

Apart from that, after treatment systems are getting more complex, increasing the number of parameters and, thus, project complexity. This also increases development time, since more combinations have to be tested.

One well known way of reducing development time and costs is the use of computer simulations. Since an engine could be described as a device for converting energy stored (contained) in a fluid to mechanical energy, fluid dynamics simulations is the topic of concern here. However, since engine phenomena involve turbulence and combustion, three-dimensional CFD (computer fluid dynamics) becomes prohibitive when one wants to have a broader view of the technological landscape or study the influence of several parameters, since either long simulation times or too much computational power would be needed (Kaechele *et al.*, 2018).

To overcome this difficulty, the so called 1D/0D simulation models are used by engine developers. Basically, the fluid mixture (air, air/fuel mixture or burned gas) is considered homogeneous along the pipes' cross-sections. Fluid properties change only along flow direction (thus, the one-dimensional 1D classification). In the combustion chamber, fluid is divided in two zones: burned and unburned. During combustion, mass is transferred from the unburned zone to the burned zone. Composition, pressure and temperature are considered homogeneous in each of the two zones, thus the zero-dimensional

0D classification.

Heywood (1988) discusses CO and NO equilibrium and kinetic models which can be easily coupled in such 1D/0D simulations to predict emissions, without the need of detailed combustion chamber characteristics. Comparisons with experimental data are provided and simulations are used to discuss the main factors influencing emissions of these two pollutants.

Raggi and Sodré (2014) used a research engine running on iso-octane to calibrate a kinetic CO model. Results from both kinetic and equilibrium (developed in a previous work) were compared with the research engine experimental results for a wide range of air/fuel ratio values. The results of kinetic model had 7% maximum deviation to experimental results, while the equilibrium model reached 50% deviation. In this case, the equilibrium model was only capable of predicting CO emissions for lean mixtures. The CO models (both equilibrium and kinetics) were then validated using results of a production, four-cylinder, 16-valve, 1.0l engine, running on E22 and for a variety of engine speed and throttle positions. The maximum discrepancies found between the kinetic and the equilibrium CO values in comparison to the experimental results from the production engine were 11.5% and 15.4%, respectively. The authors conclude the kinetic model gave more accurate results for rich mixture operation, but for stoichiometric and lean operation, both models presented similar results.

Niculae *et al.* (2019) also used gasoline experimental data to calibrate kinetic emissions models. However, not only CO, but also HC and NO were measured and simulated. The data included two lambda values (1 and 1.25) and several spark ignition timings at a single operating point (2000 rpm and 2 bar bmep). For each condition, different coefficients values were employed to adjust the emissions models. The calibrated simulation results matched the experimental data with a maximum 1% error (except for two particular points with lambda 1.25). The same coefficients values were then used to simulate the same engine running on different mixtures of hydrogen and natural gas, these mixtures being called hythane. The paper also used the same imposed combustion parameters (start of combustion, burn duration) for all fuels. No correlation with experiments was presented for the hythane simulations, being this correlation left as future work.

Hann *et al.* (2020) used a kinetic NO model to predict emissions in a large power generation application CNG engine running with different lambda, intake manifold air temperature (IMAT) and MFB50 values. The model uses a predictive combustion model and only needs four points for model calibration. A factor of 6.2 was necessary to match NO emissions. Here it is important to point out that the model is only capable of predicting NO, but the experimental measurements lump both NO and NO_2 values under NOx. The high coefficient value aims at compensating this difference, as well as other inaccuracies. There is a good match for high lambda values. For lower lambda values, the model overestimates NOx values. One possible explanation, given by the paper, is the variation of the NO_2/NO ratio with lambda. Since the model doesn't predict NO_2, this would explain the discrepancies between model and experiment. Another possible explanation would be inaccuracies in the combustion model. Only four points were used for combustion model calibration. Although a good visual match of pressure traces (for the four calibration points) and a maximal of 4% deviation in ISFC (indicated specific fuel consumption) are shown, inaccuracies in predicted combustion temperature could lead to different NO emissions results. But the general emissions trend could be successfully captured by the model, showing such simulations could and should be used to save test bench time and costs.

Instead of using predictive combustion models, Albrecht *et al.* (2020) used measured in-cylinder pressure traces and a three pressure analysis (TPA) model to calculate burn rates of an engine running on EU6 gasoline fuel. These burn rates were then imposed in a full engine model to calculate NO emissions for different fuels. All simulations were run at 2000rpm and lambda 1, but with different loads. One advantage of this approach is that more realistic cylinder conditions (pressure and temperature) are expected with the calculated burn rates. On the other hand, this requires more experimental data, which is sometimes not available. Additionally, using the same burn rate for different fuels might not be representative of the real engine conditions (different fuels have different laminar flame speeds (Kuo, 2005), for instance), but it definitely can help in a first guess, when not enough data is available.

In this paper, the accuracy of CO and NO kinetic models, coupled with a 1D/0D engine model, is going to be evaluated, through the comparison of simulation results with test bench data from a 3 cylinder, 1.2 liter turbocharged direct injection spark ignition (DISI) engine, running on E10.

2. METHODOLOGY

In order to evaluate the models mentioned in Introduction, a PSA EB2 PureTech engine (Souhaite and Mokhtari, 2014) (1.2l three-cylinder turbo direct injection (DI) spark ignition (SI)) was installed in an engine dynamometer. The main engine characteristics are shown in Tab. 1. The measurement data was used to calibrate an one-dimensional (1D) model of the engine and calculate the respective burn rates. Using the calibrated model and calculated burn rates, emissions were then simulated and correlated with the measurements. The next sections describe further details of both dynamometer measurements and simulation model.

Table 1. Engine characteristics

Number of cylinders	3
Cylinder bore	75.00 mm
Piston stroke	90.50 mm
Engine displacement	1199 cm^3
Crankshaft radius	45.17 mm
Crankshaft offset	7.5 mm
Connecting rod length	144.0 mm
Nominal compression ratio	10.5:1
Max power	96 kW @ 5500 rpm
Max torque	230 Nm @ 1750 rpm
Fuel system	Direct Injection, 200 bar Up to 3 injections per cycle
Turbocharger system	Single scroll turbocharger Max. boost-pressure 1.4 bar Max. speed 270000 rpm.
Oil pump	Sensored regulation oil pump
Cylinder head	Integrated exhaust manifold 4 valves/cylinder (2 int. 2 exh.)
Timing System	Dual variable valve timing IVO = -30 / 40 °CA @ 1mm lift EVO = -35 / 35 °CA @ 1mm lift

2.1 Experimental Setup

The engine was coupled to a passive eddy current, water cooled, Positron Brown-Boveri brake, capable of running at maximum speed of 9000 rpm and maximum torque of 750 N.m. A torque flange HBM model T40B, nominal capacity of 1000 N.m and 20000 rpm, was installed between engine and brake to measure engine torque. Air and fuel consumption were measured using a hot wire flow meter model Contech FT2 for air flow measurement and a Coriolis flow meter model MicroMotion CMF010M for fuel flow. Table 2 shows relevant measured quantities and their source. Figure 1 shows a schematic diagram of the engine installation.

Table 2. Measured quantities and their source

Variable	Source
Air mass flow	Hot wire flow meter
Fuel flow	Coriolis flow meter
Injection timing	ECU
Injected mass split (among pulses)	ECU
Cooling water temperature	ECU
Oil pan temperature	K-type thermocouple
Intake manifold temperature	K-type thermocouple
Exhaust temperature	K-type thermocouple
Spark timing	ECU
Valve timing (intake and exhaust)	ECU
Humidity	Vaisala HTM130
Ambient temperature	Vaisala HTM130
Intake manifold pressure	Fast sensor
Exhaust pressure	Fast sensor
In-cylinder pressure	Fast sensor
Crank angle	AVL 365C angle encoder

Three fast pressure sensors, capable of measuring crank angle resolved values, were mounted at cylinder 3: two Kulite XTL 190 - 205 DC, with external cooling, one at each port (depicted as P1 at intake and P3 at exhaust in Fig. 1) and one water-cooled piezoelectric, model Kistler 6041BS32 for in-cylinder pressure (P2 in Fig. 1). In order to synchronize the pressure traces to the engine operation, an AVL 365C angle encoder was mounted at the crankshaft.

For raw exhaust emission (pre-catalyst) measurements, a Horiba MEXA 200 was employed.

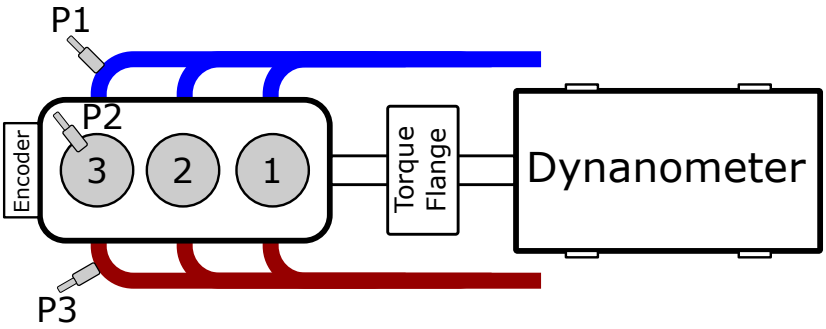

Figure 1. Schematic diagram of engine and sensors installation

Table 3 shows the operating points used in this work. This is a full load curve for engine speeds from 1000 rpm to 6000 rpm, in 500 rpm intervals. For each operating point, 150 cycles were measured. Cycle quantities (air flow, fuel flow, BMEP, IMEP, BSFC, emissions) were averaged among these cycles. The pressure traces were recorded individually for each of cycle.

Table 3. Measured operating points

Engine speed (rpm)	BMEP (bar)	Engine speed (rpm)	BMEP (bar)
1000	12	4000	22
1500	22	4500	18
2000	22	5000	18
2500	24	5500	18
3000	24	6000	16
3500	22		

2.2 Simulation Model

The engine simulation model was built and solved using a well known commercial engine simulation software called GT-Power (Gamma Technologies, 2019a). GT-Power uses the already described 1D/0D modelling approach. The whole system is discretized into individual volumes, which are connected by boundaries. Scalar variables (pressure, temperature, density, internal energy, enthalpy, species concentrations, etc.) are considered uniform over each volume. Vector variables (mass flux, velocity, mass fraction fluxes, etc.) are calculated for each boundary.

The continuity (Eq. (1)), energy (Eq. (2)), enthalpy (Eq. (3)) and momentum (Eq. (4)) equations (shown below) are then solved. These equations are solved in one dimension, which means that all quantities are averages across the flow direction (Gamma Technologies, 2019c).

$$\frac{dm}{dt} = \sum_{boundaries} \dot{m} \tag{1}$$

$$\frac{d(me)}{dt} = -\rho\frac{dV}{dt} + \sum_{boundaries} (\dot{m}H) - hA_S(T_{fluid} - T_{wall}) \tag{2}$$

$$\frac{d(\rho HV)}{dt} = \sum_{boundaries} (\dot{m}H) + V\frac{dp}{dt} - hA_S(T_{fluid} - T_{wall}) \tag{3}$$

$$\frac{d\dot{m}}{dt} = \frac{dpA + \sum_{boundaries}(\dot{m}u) - 4C_f\frac{\rho u|u|}{2}\frac{dxA}{D} - K_p\left(\frac{1}{2}pu|u|\right)A}{dx} \tag{4}$$

where:

$\dot{m}$	boundary mass flux into volume	m	mass of the volume
V	volume	p	pressure
ρ	density	A	cross-sectional flow area
A_s	heat transfer surface area	e	total specific internal energy
H	total specific enthalpy	h	heat transfer coefficient
T_{fluid}	fluid temperature	T_{wall}	wall temperature
u	velocity at the boundary	C_f	Fanning friction factor
K_p	pressure loss coefficient	D	equivalent diameter
dx	length of mass element in the flow direction	dp	pressure differential acting across dx

The cylinder is simulated as a single homogeneous volume, separated in two zones: the unburned zone, containing a mixture of fuel and air, and the burned zone, whose composition is calculated using a burn rate and a combination of chemical equilibrium and kinetics. In the particular case of this paper, in order to more accurately predict in-cylinder composition (in this case, the residual burned gas fraction), a so called TPA (three pressure analysis) model was built. TPA models contain only one cylinder and its intake and exhaust ports. The measured intake and exhaust pressure traces were imposed at the respective boundaries of the model (ports). Using the measured in-cylinder pressure and the simulation, it is possible to calculate the burn rate (i.e. the rate at which fuel mass is oxidized) by solving the energy equation for the contents of the cylinder (Gamma Technologies, 2019b):

$$\frac{d(me_f)}{dt} - \sum_{boundaries} \dot{m}H_f = -p\frac{dV}{dt} - \frac{dQ}{dt} - \frac{d(me_s)}{dt} + \sum_{boundaries} \dot{m}H_s \tag{5}$$

where:

e_f	internal formation energy
e_s	internal sensible energy
H_f	formation enthalpy
H_s	sensible enthalpy
Q	heat transfer (fluid to wall)

In a first step, this methodology was used to calculate the burn rate for each measured operating point. Then, in a second step, the reversed methodology was applied: the calculated burn rate profiles were imposed and in-cylinder pressure trace calculated, using the same Eq. (5). The only difference is that, now, burn rate is an input and in-cylinder pressure an output.

More specifically, the imposed burn rate defines the rate at which fuel/air mixture is moved from the unburned zone to the burned zone. Then, using in-cylinder calculated conditions from the previous time step (pressure, temperature, composition), chemical equilibrium and kinetics calculations are performed to determine the reactants break down into products of combustion (both intermediate and final). Finally, using this newly calculated in-cylinder composition, the heat release rate is calculated for the current time step, leading to new in-cylinder pressure and temperature values.

Injected fuel mass was calculated to reproduce the exact same air/fuel ratio from experimental data, which was calculated using the measured air and fuel flow. Thus, even if the air flow doesn't exactly match the experiments, the air fuel mixture composition will be preserved. However, one important characteristic of this particular engine is the early intake valve opening (thus, longer valve overlap) at low engine speeds, which leads to high scavenging and high exhaust lambda measurements (Souhaite and Mokhtari, 2014), which differs from combustion (trapped in the cylinder) lambda for these operating points. In other words, the trapped air/fuel ratio at IVC cannot be guaranteed for the low engine speed operating points, nor compared to experimental data. But, if air flow is matching experimental data and if the valve flow coefficients are correctly calibrated, it is expected that the model would be able to accurately calculate the trapped composition.

In order to calculate brake quantities (power, torque and BMEP (break mean effective pressure)), a FMEP (friction mean effective pressure) lookup table having engine speed and oil temperature as inputs was used as engine friction model.

2.2.1 CO Emissions Calculation

For CO emissions calculation, the following kinetic mechanism was used (Bowman, 1975):

$$\mathrm{CO} + \mathrm{OH} \rightleftharpoons \mathrm{CO_2} + \mathrm{H} \tag{6}$$

The rate constant for the forward reaction is given by:

$$K_{forward} = A \cdot 6.76 \cdot 10^7 \cdot e^{T_b/B \cdot 1102} \tag{7}$$

where:

A	pre-exponent multiplier
B	activation temperature multiplier
T_b	burned sub-zone temperature (K)

The rate constant is in $m^3/(kg \cdot mol)$ units. Both A and B multipliers were kept at their default values: 1. The rate constant for the reverse reaction is calculated from equilibrium constant, which is calculated from thermodynamics.

2.2.2 NO Emissions Calculation

For NO emissions calculation, the extended Zeldovich kinetic mechanism was used (Lavole *et al.*, 1970):

$$\mathrm{O} + \mathrm{N_2} \rightleftharpoons \mathrm{NO} + \mathrm{N} \tag{8}$$

$$\mathrm{N} + \mathrm{O_2} \rightleftharpoons \mathrm{NO} + \mathrm{O} \tag{9}$$

$$\mathrm{N} + \mathrm{OH} \rightleftharpoons \mathrm{NO} + \mathrm{H} \tag{10}$$

The respective rate constants for the forward reactions are given by:

$$K_8 = F_1 \cdot 7.60 \cdot 10^{10} \cdot e^{-38000 \cdot A_1/T_b} \tag{11}$$

$$K_9 = F_2 \cdot 6.40 \cdot 10^{6} \cdot T_b \cdot e^{-3150 \cdot A_2/T_b} \tag{12}$$

$$K_{10} = F_3 \cdot 4.10 \cdot 10^{10} \tag{13}$$

where:

F_1	N2 oxidation rate multiplier	A_1	N2 oxidation activation energy multiplier
F_2	N oxidation rate multiplier	A_2	N oxidation activation energy multiplier
F_3	OH reduction rate multiplier	T_b	burned sub-zone temperature (K)

All rate constants are in $(m^3/kmol \cdot sec)$ units. All multipliers (F_1, F_2, F_3, A_1 and A_2) were kept at their default values: 1. The reverse reaction constants are calculated from the respective equilibrium constants, which are calculated from thermodynamics.

This mechanism is not able to predict NO_2. However, spark ignition engines are known to have most of its NOx emissions in the form of NO (Heywood, 1988).

3. RESULTS

As explained, two different sorts of simulations were run: one to calculate burn rate, and another one to calculate emissions, using the previously calculated burn rate. The results presented here are from the latter simulation run.

3.1 Base Quantities

Figure 2 shows the deviation in air flow between simulation and experiment. There is a good agreement in general, with error ranging from -5% and 5%, except for the 1500 rpm point.

Figure 3 shows the deviation in IMEP and BMEP between simulation and experiment. As can be seen, IMEP has a better match to experimental results, but some discrepancies are still observed. IMEP deviations will be discussed first, since they involve deviations in in-cylinder pressure, which is a very important quantity for this work. BMEP deviations will be discussed right after.

Since air flow matched quite well, IMEP comparison is an indication of how well the in-cylinder pressure is being reproduced by the model. From 3500 rpm onwards, the simulation is predicting less IMEP than measured at the engine. Two other important quantities when dealing with in-cylinder pressure are peak cylinder pressure and peak cylinder pressure location (Fig. 4). Peak cylinder pressure location was well predicted by the model, but the peak cylinder pressure values seem to explain the deviation in IMEP values, since it has the same trend.

In order to have a closer look at the IMEP deviation, Fig. 5 shows a comparison between simulated and measured cylinder pressure traces for the 4500 rpm 18 bar operating point, the one with the highest peak cylinder pressure deviation and having one of the worst IMEP correlations to experiment. Simulated pressure values in high pressure loop are always lower than the measured values, although the general trend is well predicted. Since pumping loop and air flow rate have good correlation (less than 2% deviation in air flow), two possible explanations would be in-cylinder heat transfer or the rate of heat release calculation. However, the main important conclusion from this plot is that the burning rate seems to be well predicted, since the in-cylinder pressure didn't present any local big deviations to test data. Although some deviation in in-cylinder temperature can be expected (something that has a direct impact in chemical kinetics), the general trend is

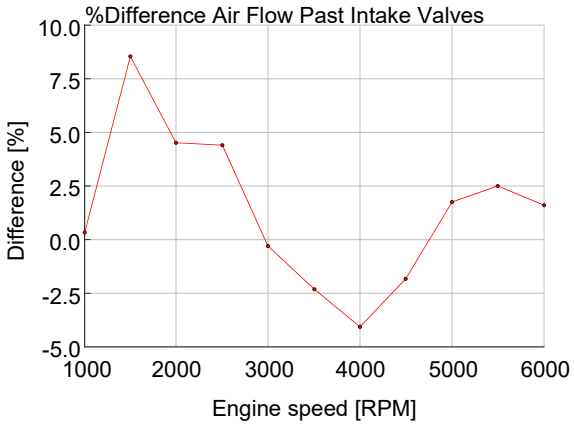

Figure 2. Air flow deviation to test data

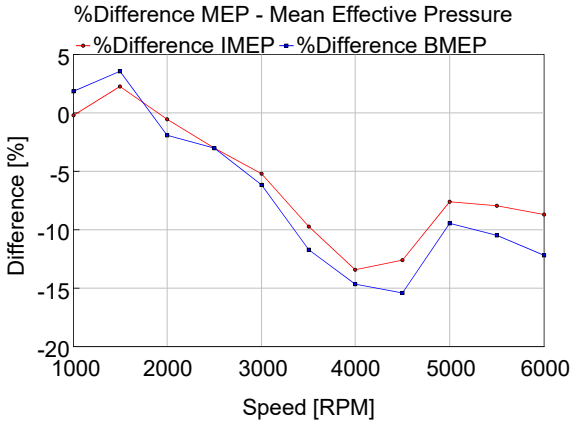

Figure 3. IMEP and BMEP deviation to test data

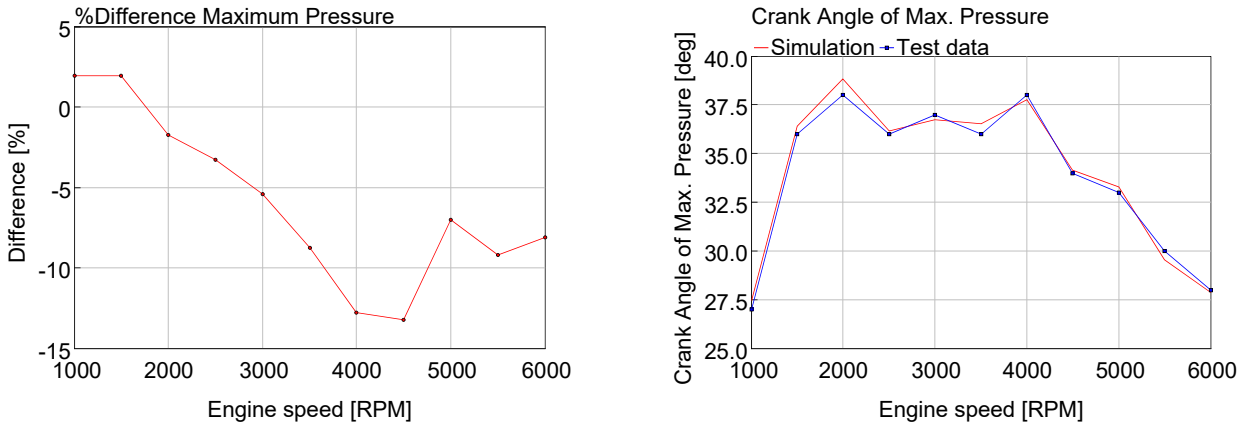

Figure 4. Peak cylinder pressure (left) and peak cylinder pressure location (right) comparison to test data.

there in the model.

The pressure traces from other operating points had a similar correlation or even better, and won't be shown here for the sake of space.

As already pointed out, the BMEP deviation is even higher than the one observed for IMEP. Concerning simulation results, FMEP error and IMEP error are added to compose BMEP error. However, concerning test data, BMEP comes

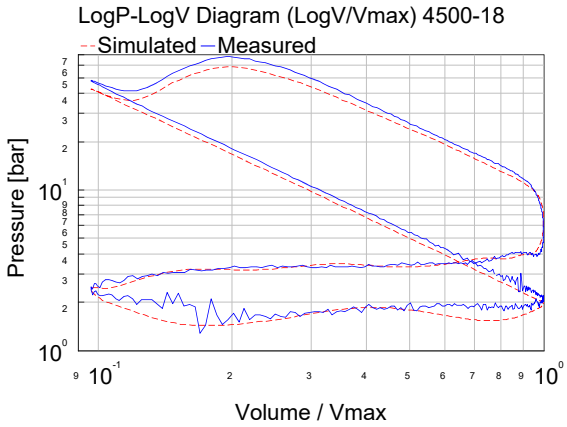

Figure 5. Cylinder pressure trace comparison to test data (4500rpm-18bar)

from a completely different source: the measured torque at the torque flange. The measured pressure trace (used in IMEP's computation) is not used at BMEP's calculation in the test data. Thus, the difference between IMEP's and BMEP's deviation could come from:

1. Modeled FMEP error.
2. Inconsistency between measured break torque and in-cylinder pressure (or its phasing).

Since the measured in-cylinder pressure error has a direct impact in the simulation error (it was used to calculate the burn rates used in the simulation) and to keep comparisons in the same basis, it was decided to present the rest of the results in this paper using indicated quantities as reference.

3.2 CO Emissions

Figure 6 shows an indicated specific CO emissions comparison between simulation and test data, showing both absolute and percent difference values. The lower engine speed points present the higher differences. Those are also the points with the least emissions, thus, even small absolute deviations can lead to very high percent deviations. From 3000 rpm onwards, a deviation of around 40% is present for all points. Even with the very high percent error for the low engine speeds, the general trend could be predicted for the whole full load curve.

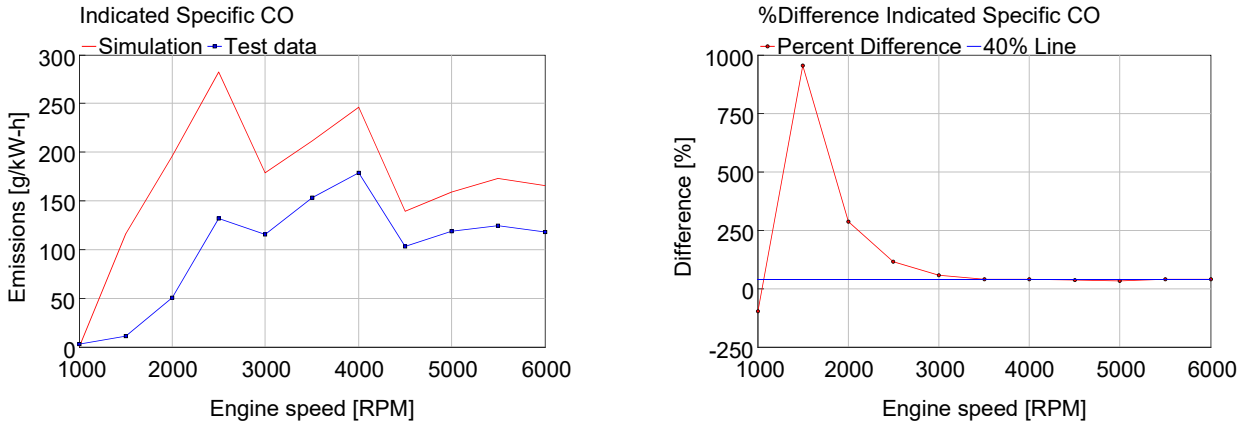

Figure 6. Indicated specific CO emissions comparison (left: absolute; right: percentage) to test data

According to Heywood (1988), carbon monoxide emissions in internal combustion engines are primarily controlled by equivalence ratio. One possible explanation for the difference at low engine speed points would be a deviation of trapped lambda between model and experiment, since this engine presents high scavenging at these points, as already mentioned in Methodology. Since trapped lambda couldn't be measured, only exhaust lambda was imposed in the model. Inaccuracies at valve coefficients could thus lead to such deviations in the trapped quantities.

Another possible (and more likely, in this case) source of deviations is the fact that the model considers the combustion chamber as a homogeneous mixture, which not necessarily represents the real engine. One possible way to overcome these deviations would be to calibrated the pre-exponent and activation temperature multipliers in the rate constants for the kinetic mechanisms, which were kept at 1 in this work.

3.3 NOx Emissions

Figure 7 shows an indicated specific NO emissions comparison between simulation and test data, showing both absolute and percent difference values. In general, the deviations are smaller than for CO predictions. Except for the 1000 rpm point, the model tends to predict less NOx than the test. This might be explained by the fact that NO_2 is being measured, but not simulated, as already mentioned in the Methodology. This wouldn't explain the high percentage values though, but since the absolute emissions values are quite low, any small deviation could lead to high percentage deviation values, as observed.

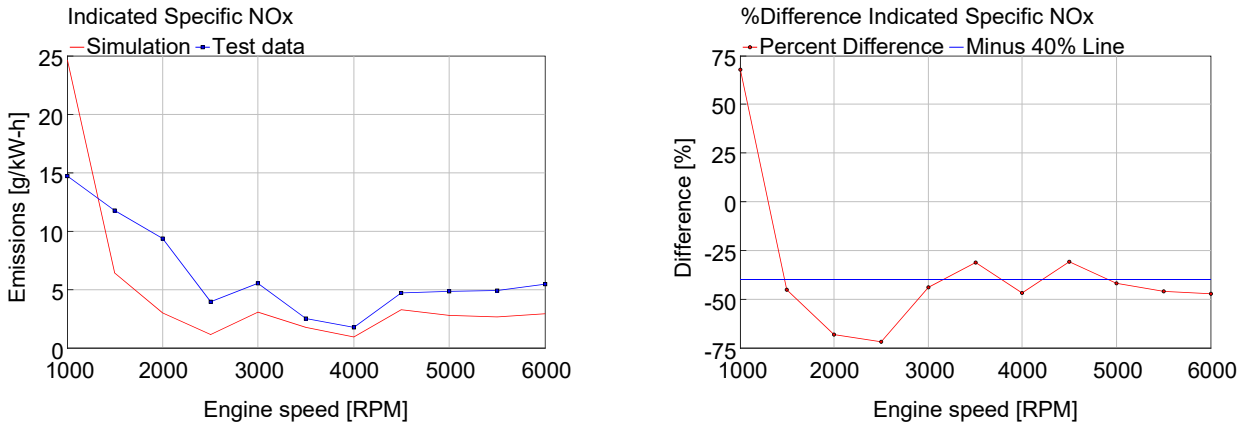

Figure 7. Indicated specific NO emissions comparison (left: absolute; right: percentage) to test data

As far as deviations to test data go, the same considerations stated for CO emissions are applicable here: combustion lambda is one possible source of deviation, as well as combustion chamber homogeneity. However, another important quantity for NO emissions is combustion temperature, which was also not measured. This is another possible source of deviations.

Comparing both simulation and test data, CO and NOx emissions trends are opposite, as expected (Kuo, 2005). CO tends to form in rich mixtures and NOx requires leaner environments. Therefore, an increase in one of the pollutants should be coupled with a decrease in the other, which is observed in both simulation and test data.

4. CONCLUSIONS

This work's objective was to evaluate how well simple zero-dimensional kinetic models could predict CO and NO emissions. A reduced (one cylinder) engine model was built. Using this model, the burn rate profiles of eleven full load operating points were calculated. These profiles were than imposed in the model, and the kinetic emissions models for CO and NO were turned on, with parameters in default values (i.e. no kinetic model calibration). Low engine speed points had the higher deviations for both CO (predicting up to 10 times the measured value) and NOx (overestimation of 67% for 1000 rpm and up to 70% underestimation for 2500 rpm). One possible source of inaccuracy for this points is the difference between combustion lambda (considering trapped quantities) and exhaust lambda (considering total fuel and air flow), being the former not measurable. These points have early intake vale opening, leading to intake and exhaust short circuit, which then leads to the combustion and exhaust lambda difference. Another possible source of inaccuracy is the combustion chamber homogeneity assumption, which not necessarily represents the real engine.

For the rest of the engine speed range, the deviations were lower, but still considerable (around 40% overestimation for CO and between 25% and 50% underestimation for NOx). Although the measured values could not be accurately predicted, the general trend was captured, with CO being always overestimated and NOx underestimated. CO and NOx emissions trends were opposite, as expected. As suggestions for next steps, the kinetics models should be calibrated taking all measured data into consideration, perhaps separating between calibration and validation operating points. A NO_2 kinetics model should also be included to check if a better match to experimental data could be achieved.

5. ACKNOWLEDGEMENTS

The authors want to thank São Paulo Research Foundation (FAPESP), grant #2013/50238-3, and PSA Groupe for the technical and financial support in this project, as part of the activities of Prof. Urbano Ernesto Stumpf Research Center.

6. REFERENCES

ABNT, 2012. "Veículos rodoviários automotores leves — Determinação de hidrocarbonetos, monóxido de carbono, óxidos de nitrogênio, dióxido de carbono e material particulado no gás de escapamento". Standard, ABNT. doi: 01.080.10; 13.220.99.

Albrecht, M., Deeg, H.P., Schwarzenthal, D. and Eilts, P., 2020. "Investigations of the Emissions of Fuels with different Compositions and Renewable Fuel Components in a GDI Engine". In *SAE Technical Papers*. April, pp. 1–8. ISSN 01487191. doi:10.4271/2020-01-0285. URL https://www.sae.org/content/2020-01-0285/.

Bowman, C.T., 1975. "Kinetics of pollutant formation and destruction in combustion". *Progress in Energy and Combustion Science*, Vol. 1, No. 1, pp. 33–45. ISSN 03601285. doi:10.1016/0360-1285(75)90005-2.

Gamma Technologies, 2019a. "Gamma Technologies | The Standard in Multi-Physics System Simulation". URL https://www.gtisoft.com/.

Gamma Technologies, 2019b. "GT-SUITE Engine Performance Application Manual".

Gamma Technologies, 2019c. "GT-SUITE: Flow Theory Manual".

Hann, S., Palaveev, S., Grill, M., Veltman, M. and Bargende, M., 2020. "Predicting the Influence of Charge Air Temperature Reduction on Engine Efficiency, CCV and NOx-Emissions of a Large Gas Engine Using a SI Burn Rate Model". *SAE Technical Papers*, Vol. 2020-April, No. April, pp. 1–18. ISSN 01487191. doi:10.4271/2020-01-0575.

Heywood, J.B., 1988. *Internal combustion engine fundamentals*. McGraw-Hill. ISBN 9781260116106. doi: 10.5860/choice.26-0943.

Kaechele, A., Chiodi, M. and Bargende, M., 2018. "Virtual Full Engine Development: 3D-CFD Simulations of Turbocharged Engines under Transient Load Conditions". *SAE International Journal of Engines*, Vol. 11, No. 6, pp. 697–714. ISSN 19463936, 19463944. doi:10.2307/26649125. URL https://www.jstor.org/stable/26649125 http://www.jstor.org/stable/26649125.

Kuo, K.K., 2005. *PRINCIPLES OF COMBUSTION SECOND EDITION*. John Wiley & Sons Inc, New York, United States, 2nd edition. ISBN 978-0-471-04689-9. URL http://as.wiley.com/WileyCDA/WileyTitle/productCd-0471046892.html.

Lavole, G.A., Heywood, J.B. and Keck, J.C., 1970. "Experimental and theoretical study of nitric oxide formation in internal combustion engines". *Combustion Science and Technology*, Vol. 1, No. 4, pp. 313–326. ISSN 1563521X. doi:10.1080/00102206908952211. URL https://www.tandfonline.com/doi/abs/10.1080/00102206908952211.

Niculae, A.L., Miron, L. and Chiriac, R., 2019. "On the possibility to simulate the operation of a SI engine using alternative gaseous fuels". In *Energy Reports*. Elsevier Ltd, Vol. 6, pp. 167–176. ISSN 23524847. doi: 10.1016/j.egyr.2019.10.035.

Raggi, M.V.K. and Sodré, J.R., 2014. "Numerical simulation of carbon monoxide emissions from spark ignition engines". *Journal of the Brazilian Society of Mechanical Sciences and Engineering*, Vol. 36, No. 1, pp. 37–43. ISSN 16785878. doi:10.1007/s40430-013-0076-0.

Souhaite, P. and Mokhtari, S., 2014. "Combustion system design of the new PSA Peugeot Citroën EB TURBO PURE TECH engine". In *Internationaler Motorenkongress*. pp. 49–72. doi:10.1007/978-3-658-05016-0_5. URL http://link.springer.com/10.1007/978-3-658-05016-0_5.

Vitesco Technologies, 2019. "Worldwide Emission Standards and Related Regulations". Technical report, Vitesco Technologies. URL www.continental-automotive.comPowertrain.

7. RESPONSIBILITY NOTICE

The authors are solely responsible for the printed material included in this paper.